We are not the 99 percent: quantifying asphericity in the distribution of Local Group satellites

Jaime E. Forero-Romero [1] *, Verónica Arias[1]
[1] *Departamento de Física, Universidad de los Andes, Cra. 1 No. 18A-10 Edificio Ip, CP 111711, Bogotá, Colombia*

1 May 2018

ABSTRACT
We use simulations to build an explicit probability distribution for the asphericity in the satellite distribution around Local Group (LG) type galaxies in the Lambda Cold Dark Matter (LCDM) paradigm. We use this distribution to estimate the atypicality of the satellite distributions in the LG even when the underlying simulations do not have enough systems fully resembling the LG in terms of its typical masses, separation and kinematics. We demonstrate the method using three different simulations (Illustris-1, Illustris-1-Dark and ELVIS) and a number of satellites ranging from 11 to 15. Detailed results differ greatly among the simulations suggesting a strong influence of the typical DM halo mass, the number of satellites and the simulated baryonic effects. However, there are three common trends. First, at most 2% of the pairs are expected to have satellite distributions with the same asphericity as the LG; second, at most 80% of the pairs have a halo with a satellite distribution as aspherical as in M31; and third, at most 4% of the pairs have a halo with satellite distribution as planar as in the MW. These quantitative results place the LG at the level of a 3σ outlier in the LCDM paradigm. We suggest that understanding the reasons for this atypicality requires quantifying the asphericity probability distribution as a function of halo mass and large scale environment. The approach presented here can facilitate that kind of study and other comparisons between different numerical setups and choices to study satellites around LG pairs in simulations.

Key words: Cosmology: Dark Matter — Galaxies:Local Group — Methods: numerical

1 INTRODUCTION

The spatial distribution of satellite galaxies around our Milky Way (MW) and the M31 galaxy is becoming a stringent test for structure formation theories in an explicit cosmological context. This started with the suggested existence of a Magellanic Plane, a flattened structure of satellite galaxies and globular clusters around the MW, by Kunkel & Demers (1976) and Lynden-Bell (1976). Forty years later Kroupa et al. (2005) quantified that the highly planar distribution of the 11 classical MW satellites has less than a 0.5% chance to happen by chance if the parent distribution is spherically symmetric, interpreting this as a challenge to the Lambda Cold Dark Matter (LCDM) paradigm. The same year it was recognized, using numerical simulations, that this comparison was unfair given that Dark Matter halos in LCDM are expected to be triaxial and not spherical. Nevertheless, some estimates of the chances to find simulated satellites as planar as in the MW were as low as 2% (Zentner et al. 2005) while others expected planar satellite configurations in every DM halo (Libeskind et al. 2005).

Later, Metz et al. (2007) used simulations to confirm the low chances ($< 0.5\%$) found in Kroupa et al. (2005). This result was challenged by Libeskind et al. (2009) who continued to report high chances to find a planar configuration; two more recent numerical experiments with high resolution simulations (Starkenburg et al. (2013) and Sawala et al. (2016)) reported contradicting results (low and high chances to find the observational result, respectively) but precise figures were not quoted in these three reports. Meanwhile, Wang et al. (2013) and Pawlowski & McGaugh (2014) published the results of new tests using high resolution simulations and cosmological volumes arriving at a chance of 6% and 0.77%, respectively, to have a satellite distribution as triaxial as the observations.

In the case of M31, all studies agree on the point that the spatial distribution of the 15 to 27 brightest satellites are consistent with spherically symmetric distributions and easy

to reproduce in LCDM simulations (Koch & Grebel 2006; Metz et al. 2007; Conn et al. 2013). In a very different observational statement, there is a subset of 15 satellites out of the total population of 27 satellites that show a highly planar distribution (Conn et al. 2013; Ibata et al. 2013; Collins et al. 2015). This so-called satellite plane is deemed to be difficult to produce in LCDM simulations and is thought to be transient structure (Cautun et al. 2015; Buck et al. 2015; Gillet et al. 2015; Buck et al. 2016; Ahmed et al. 2017; Fernando et al. 2017). However, in this paper we do not address these *plane finding* algorithms and focus instead on the characterization of the global satellite distribution ranked either by decreasing luminosity, maximum circular velocity or stellar mass. Table 1 and Table 2 summarize some more details on the results we have just mentioned [1].

Some of the difficulty in trying to reconcile and understand the seemingly conflicting or inconclusive results on the MW has its origin on the frequentist fashion generally used to compute probabilities. Usually, this process starts by building a high level parent sample in the simulation and then counting how many elements has the subset meeting some criteria. This has two inconveniences. The first is that the probability estimate is made against whatever turns out to be typical in each simulation. A fair comparison across simulations would require first characterizing all the simulations at the high level parent samples, something that is difficult to do in practice. The second inconvenient is that the systems that fully resemble the LG (i.e. its stellar mass content, morphology or kinematics) have a low cosmological number density (Forero-Romero et al. 2013), this means that for the current cosmological volumes in simulations the high level parent sample has a small size, making it hard to derive robust probabilities by counting. In this paper we present and demonstrate a method to overcome these two limitations.

We control the first effect by setting as a direct point of reference a spherical satellite distribution and not the simulations themselves. The spherical satellite distribution is built from the data itself (observational or simulated) by randomizing the angular position of each satellite around the central galaxy and keeping its radial distance fixed (Pawlowski et al. 2017). We characterize the satellites in terms of the scalars describing its deviation from the spherical distribution. We then build an explicit analytic probability distribution for the asphericity; this solves the problem of having a common reference point to compare simulations. We use a simulation to estimate the parameters in this distribution to later use it as a parent sample to generate any desired number of samples that are by construction statistically compatible with the simulation; thus overcoming the problem of having a small number of systems in the parent simulations.

To summarize, we use asphericity to characterize on equal footing simulations and observations. Then, we build an analytical probability distribution for the asphericity and use simulations to estimate its free parameters. Finally, we use these distributions to generate large numbers of samples and directly estimate the number of systems meeting a desired set of criteria.

The rest of the paper describes in detail our implementation and results. It is structured as follows. In Section 2 we list the sources of the observational and simulated data to be used throughout the paper. In Section 3 we describe the methods we use to build halo pairs and characterize their satellite distributions. In Section 4 we present our results to finally conclude in Section 5.

2 DATA SAMPLES

2.1 Observational Data

The base for our analysis is the catalog compiled by Pawlowski et al. (2014) which reports information on all galaxies within 3 Mpc around the Sun to that date. Detailed description of the compiled catalog can be found in Pawlowski et al. (2013), here we summarize the relevant features for the current study. The information in the catalogue is based on the catalogue compiled by McConnachie (2012). The distance estimates are based on resolved stellar populations. We use three dimensional positions in a cartesian coordinate system as computed by Pawlowski et al. (2013). In this coordinate system the z-axis points towards the Galactic north pole, the x-axis points in the direction from the Sun to the Galactic center, and the y-axis points in the direction of the Galactic rotation.

For both the M31 and MW we only use the 11 to 15 brightest satellites (using M_V magnitudes) within a distance of 300kpc from its central galaxy. The satellites included for the MW analysis are: LMC, SMC, Canis Major, Sagittarius dSph, Fornax, Leo I, Sculptor, Leo II, Sextans I, Carina, Ursa Minor, Draco, Canes Venatici (I), Hercules and Bootes II. The satellites included for the M31 analysis are: Triangulum, NGC205, M32, IC10, NGC185, NGC147, Andromeda VII, Andromeda II, Andromeda XXXII, Andromeda XXXI, Andromeda I, Andromeda VI, Andromeda XXIII, LGS 3, and Andromeda III.

2.2 Simulated Data

We use data from three different simulations: Illustris-1, Illustris-1-Dark and ELVIS. In what follows we describe the relevant detailed of those simulations, how the halo pairs resembling the LG are selected and how the satellite samples for each halo is built. Figure A1 summarizes the physical properties (maximum circular velocities, radial velocities and separation) of the halo pairs to be used.

2.2.1 Illustris-1 and Illustris-1-Dark

We use publicly available data from the Illustris Project (Vogelsberger et al. 2014). This suite of cosmological simulations were performed using the quasi-Lagrangian code AREPO (Springel 2010). They followed the coupled evolution of dark matter and gas and includes parametrizations to account for the effects of gas cooling, photoionization, star formation, stellar feedback, black hole and super massive black hole feedback. The simulation volume is a cubic box with a 75 Mpc h^{-1} side. The cosmological parameters

---

[1] Those tables also include the results from this paper using the methodology we describe in the upcoming sections.

Reference	Target Measurement	Parent Simulation	Probability (%)
Koch & Grebel (2006)	RMS width in 15 brightest satellites	Monte Carlo satellite distributions with a power law radial distribution	$87 - 99$
Metz et al. (2007)	c/a ratio and RMS width in 16 brightest satellites	Monte Carlo from a spherical power law radial distribution	17
Conn et al. (2013)	RMS width in the 27 brightest satellites	Monte Carlo randomized satellite distribution	High
This Work	c/a ratio, b/a ratio and RMS width in 11-15 brightest satellites	27 halos from selected pairs in a cosmological N-body Dark Matter only simulation ($\sim 10^6 M_\odot$ particle mass resolution)	< 80
This Work	c/a ratio, b/a ratio and RMS width in 11-15 brightest satellites	24 halos from selected pairs in a cosmological N-body hydro simulation ($\sim 10^6 M_\odot$ particle mass resolution)	< 71
This Work	c/a ratio, b/a ratio and RMS width in 11-15 brightest satellites	12 high resolution DM only N-body simulations ($\sim 10^5 M_\odot$ particle mass resolution) of halo pairs	< 57

Table 1. Probability to find the triaxiality and/or root mean squared (RMS) width of M31 satellites in LCDM simulations.

Reference	Target Measurement	Parent Simulation	Probability (%)
Kroupa et al. (2005)	RMS width in 11 classical satellites	Monte Carlo from a spherical power law radial distribution.	< 0.5
Libeskind et al. (2005)	c/a ratio of 11 classical satellites	6 high resolution DM only N-body simulations ($\sim 10^5$ $M_\odot$ particle mass resolution).	High
Zentner et al. (2005)	c/a ratio and disk width in 11 classical satellites	3 high resolution DM only N-body simulations. ($\sim 10^6$ $M_\odot$ particle mass resolution)	2
Metz et al. (2007)	c/a ratio and RMS width in 11-13 brightest satellites	Monte Carlo from a halo triaxiality distribution from LCDM simulations	< 0.5
Libeskind et al. (2009)	c/a ratio in 11 classical satellites	436 halos from a cosmological N-body simulation ($1.3 \times 10^8 M_\odot$ particle mass)	High
Starkenburg et al. (2013)	c/a ratio in 12 brightest satellites	6 High resolution DM only N-body simulations ($\sim 10^3 M_\odot$ particle mass resolution) of individual halos	Low
Wang et al. (2013)	c/a ratio or RMS width in 11 brightest satellites	1686 halos from a cosmological DM only N-body simulation ($\sim 10^6 M_\odot$ particle mass resolution)	6 or 13
Pawlowski & McGaugh (2014)	c/a and b/a ratio in 11 classical satellites	48 high resolution DM only N-body simulations ($\sim 10^5 M_\odot$ particle mass resolution) of both halo pairs and isolated halos	0.77
Sawala et al. (2016)	c/a ratio in 11 classical satellites	12 high resolution Hydro simulation of halo pairs ($\sim 10^4 M_\odot$ particle mass resolution)	High
This Work	c/a ratio, b/a ratio and RMS width in 11-15 brightest satellites	27 halos from selected pairs in a cosmological N-body Dark Matter only simulation ($\sim 10^6 M_\odot$ particle mass resolution)	< 4
This Work	c/a ratio, b/a ratio and RMS width in 11-15 brightest satellites	24 halos from selected pairs in a cosmological N-body hydro simulation ($\sim 10^6 M_\odot$ particle mass resolution)	< 1.5
This Work	c/a ratio, b/a ratio and RMS width in 11-15 brightest satellites	12 high resolution DM only N-body simulations ($\sim 10^5 M_\odot$ particle mass resolution) of halo pairs	< 1.6

Table 2. Same as Table 1 for the MW satellites.

correspond to a ΛCDM cosmology consistent with WMAP-9 measurements (Hinshaw et al. 2013).

We extract halo and galaxy information from the Illustris-1 and Illustris-1-Dark simulations. The former includes hydrodynamics and star formation prescriptions while the latter only includes dark matter physics. These simulations have the highest resolution in the current release of the Illustris Project. Illustris-1 has 1820^3 dark matter particles and 1820^3 initial gas volume elements, while Illustris-1-Dark has 1820^3 dark matter particles. This corresponds to a dark matter particle mass of $6.3 \times 10^6 M_\odot$ and a minimum mass for the baryonic volume element of $1.2 \times 10^6 M_\odot$ for Illustris-1 and a dark matter particle mass of $7.6 \times 10^6 M_\odot$ for Illustris-1-Dark. In both simulations the dark matter gravitational softening is 1.4 kpc.

We build a sample of pairs that resemble the conditions

in the LG as follows. First, we select from Illustris-1 all the galaxies with a stellar mass in the range $1 \times 10^{10} M_{\odot} < M_{\star} < 1.5 \times 10^{11} M_{\odot}$. Then we select the pairs with the following conditions.

• For each galaxy A we find its closest galaxy B, if galaxy A is also the closest to B, the two are considered as a pair.
• With d_{AB} the distance between the two galaxies and $M_{\star,min}$ the lowest stellar mass in the two galaxies, we discard pairs that have any other galaxy C with stellar mass $M_{\star} > M_{\star,min}$ closer than $3 \times d_{AB}$ from any of the pair's members.
• The distance d_{AB} is greater than 700 kpc.
• The relative radial velocity between the two galaxies, including the Hubble flow, is -120 km s^{-1} $< v_{AB,r} < 0$ km s^{-1}.

We find 27 pairs with these conditions. In Illustris-1-Dark we use the center of mass position of the 27 pairs in Illustris-1 to find the matching halo pairs. After discarding the pairs with less than 11 detected subhalos in one of the halos we end up with a total of 24 pairs in Illustris-1-Dark. This corresponds to a pair number density of $\sim 2 \times 10^{-5}$ pairs Mpc^{-3}. Figure A1 summarizes the physical properties (maximum circular velocities, radial velocities and separation) of the halo pairs to be used.

2.3 Data from the ELVIS project

We use data from the public release of the Exploring the Local Universe In Simulations (ELVIS) project. For a detailed description of that project and its data we refer the reader to Garrison-Kimmel et al. (2014). Here we summarize the elements relevant to our discussion.

ELVIS data comes from resimulations of dark matter halo pairs selected in dark matter only cosmological simulations. The parent cosmological boxes have a cosmology consistent with the Wilkinson Microwave Anisotropy Probe 7 results. The ELVIS project used the results from 50 simulation boxes of side length 70.4 Mpc to select pairs with kinematic characteristics similar to the LG. These selection criteria included the following

• The virial mass of each host must be in the range $1 \times 10^{12} M_{\odot} < M_{vir} < 3 \times 10^{12} M_{\odot}$
• The total pair mass must be in the range $2 \times 10^{12} M_{\odot} < M_{vir} < 5 \times 10^{12} M_{\odot}$
• The center of mass separation is in the range $0.6 \leq d \leq 1$ Mpc.
• The relative radial velocity is negative.
• No halos more massive than the least massive halo within 2.8 Mpc and no halos with $M_{vir} > 7 \times 10^{13}$ within 7 Mpc of the pairs' center of mass.

This corresponds to a number density of $\sim 8 \times 10^{-6}$ pairs/Mpc^3, which is a factor ~ 2.5 lower than the pair number density we find in the Illustris-1 data. There were a total of 146 pairs that met those criteria, but only 12 were chosen for resimulation. Additionally, the selected pairs for resimulation have a relative tangential velocity less than 75km s^{-1}. The dark matter particle resolution in these resimulations is 1.9×10^5, an order of magnitude times better than Illustris-1. In this paper we only use the results from these 12 resimulated pairs.

3 BUILDING, CHARACTERIZING AND COMPARING SATELLITES SPATIAL DISTRIBUTIONS

3.1 Building Satellite Samples

We compare the joint satellite distributions in the MW and M31 at fixed satellite number, N_s. We make this choice to explicitly model the influence of satellite numbers on the statistics.

Although Illustris-1 has stellar particles, we do not use their properties to select the satellite population for the results reported here. The smallest galaxies are barely resolved in stellar mass at magnitudes of $M_V = -9$, close to the limit of the 11 "classical" MW satellites, we use instead the dark matter information.

We decide instead to use the same satellite selection rules in Illustris-1, Illustris-1-Dark and ELVIS. Namely, selecting the satellites by ranking the subhalos in decreasing order of its current maximum circular velocity and select the first N_s halos in the list.

These selection criteria also allow us to perform a fair comparison across simulations. In the case of Illustris-1 versus Illustris-1-Dark, it let us direct our attention at baryonic physics as the driver behind the differences in the results between these two simulations. To a good approximation these satellites are the systems with the highest circular velocity at infall (Boylan-Kolchin et al. 2011), which is the physical quantity expected to best correlate with luminosity (Kravtsov et al. 2004; Conroy et al. 2006; Guo et al. 2010). With this choice the maximum circular velocity cut corresponding to the smallest satellite included in the sample is different for each case; in terms of resolution the subhalos are resolved with at least $\approx 40(400)$ particles for the Illustris (ELVIS) simulation.

We compute the satellite statistics for $11 \leq N_s \leq 15$. The lower limit corresponds to the number of classical MW satellites, while the upper limit corresponds to the minimum number of satellites usually included in M31 studies. This boundary in the satellite number is also present due to the limits in the resolution of Illustris.

In observations we rank the satellites by its M_V magnitude. We also tested using M_V and stellar mass in Illustris-1, and the stellar mass in ELVIS (provided through abundance matching) as a selection criterion. Our main conclusions remain unchanged by those choices.

3.2 Describing Samples with the Inertia Tensor

We describe the satellites with the inertia tensor defined by the satellites' positions.

$$\bar{\mathbf{I}} = \sum_{i=1}^{N_p} [(\mathbf{r_i} - \mathbf{r_0})^2 \cdot \mathbf{1} - (\mathbf{r_i} - \mathbf{r_0}) \cdot (\mathbf{r_i} - \mathbf{r_0})^{\mathbf{T}}], \tag{1}$$

where k indexes the set of satellites of interest $\mathbf{r_k}$ are the satellites' positions, $\mathbf{r_0}$ is the location of the central galaxy $\mathbf{1}$ is the unit matrix, and $\mathbf{r}^T$ is the transposed vector $\mathbf{r}$. We use $\mathbf{r_0}$ as the position of the central galaxy, and not the satellites' geometrical center, to allow for a fair comparison once the angular positions of the satellites are randomized around this point.
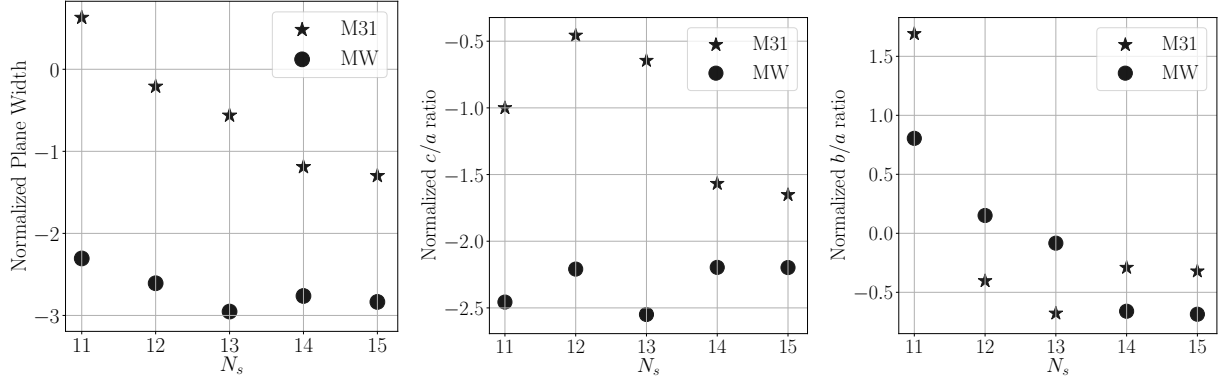
Figure 1. Normalized asphericity scalars from observations as a function of satellite number. Left: plane width; center: c/a ratio; right: b/a ratio. The plane width and c/a ratio for the MW is consistently found beyond two standard deviations. M31 shows the opposite trend and is always found *within* two standard deviations.

From this tensor we compute its eigenvalues, $\lambda_1 > \lambda_2 > \lambda_3$, and corresponding eigenvectors, $\hat{I}_1, \hat{I}_2, \hat{I}_3$. We define the size of the three ellipsoidal axis as $a = \lambda_1$, $b = \lambda_2$ and $c = \lambda_3$. We also define $\hat{n} \equiv \hat{I}_1$ as the vector perpendicular to the planar satellite distribution. We also define the Root Mean Squared (RMS) plane width w as the standard deviation of the satellite distances to the plane defined by the vector $\hat{n}$.

To summarize we characterize the satellite distribution with the following quantities obtained from the inertia tensor:

- RMS plane width, w.
- c/a axis ratio.
- b/a axis ratio.

3.3 Characterizing Asphericity

We compare each satellite distribution against its own spherically randomized distribution. We keep fixed the radial position of every satellite with respect to the central galaxy and then randomize its angular position. We repeat this procedure 10^4 times for each satellite distribution and proceed to measure the quantities mentioned in the previous section: w, c/a and b/a. This allows us to build a normalized version of all quantities of interest by subtracting the mean and dividing by the standard deviation of the values from randomized samples. We use the normalized quantities to build the explicit probability distributions for the scalars describing asphericity.

3.4 Building an explicit asphericity probability distribution

After building the normalized variables with the simulated data we perform a Kolmogorov-Smirnov test with the null hypothesis of belonging to a normal distribution with mean and standard deviation computed from the mean and standard deviation estimated from the data. Although the physical quantities of interest are bound, unlike the random variables from a normal distribution, we find that the distributions for the normalized w, c/a and b/a are indeed consistent with gaussian distributions.

Based on this result we build a multivariate normal distribution for the joint distributions of the normalized w, c/a and b/a:

$$p(X; \mu, \Sigma) = \frac{1}{(2\pi)^{3/2}|\Sigma|^{1/2}} \exp\left(-\frac{1}{2}(X - \mu)^T \Sigma^{-1}(X - \mu)\right),$$
(2)

where $X = [w, c/a, b/a]^T$ is a vector variable with the normalized quantities, μ is the vector mean and the Σ is the covariance matrix.

We compute the preferred covariance matrix and the mean distribution values with a jackknife technique. That is, out of the n pairs in each simulation, we perform n different covariance and mean value measurements using only $n - 1$ pairs. The reported covariance and mean values correspond to the average of all measurements, the corresponding standard deviation also helps us to estimate the uncertainty on every reported coefficient. This compact description allows us to generate samples of size N that are consistent by construction with their parent simulation.

Finally, we use the generated samples to estimate how common are the deviations from sphericity that we measure in the observational data. We use a double-tailed test around the mean in this comparison, meaning that we always measure the fraction of points with absolute values larger than the absolute observed value with the mean substracted.

4 RESULTS

Figure 1 shows, as a function of the number of satellites, the normalized plane width w, c/a ratio and b/a ratio from observations. The most oustanding feature of this plot is that for w and c/a ratio the MW is always two standard deviations away from the mean, while M31 is always within 2 standard deviations. The results for the b/a ratio are always 2 standard deviations both for the MW and M31. This confirms the extreme planar distribution for the MW and the more spherical distribution for the M31.

In the following subsections we describe in detail the results from Illustris-1-Dark for w, c/a and b/a for a fixed number of satellites $N_s = 11$. The results from the other
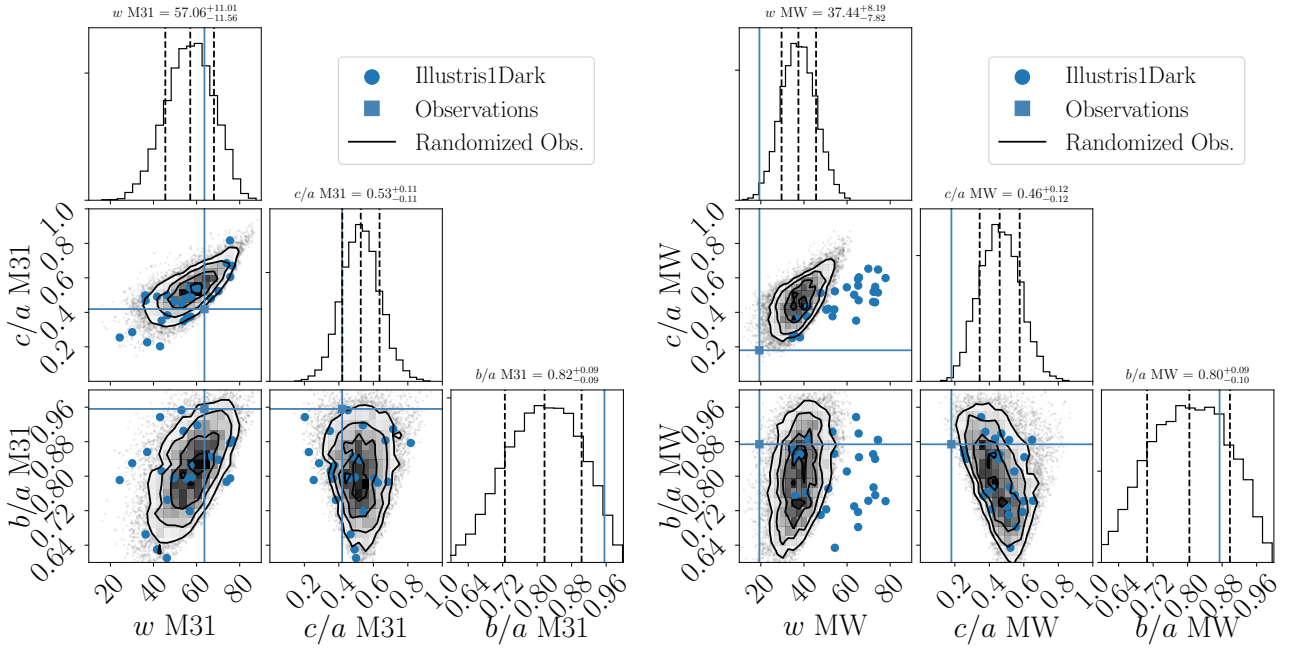
Figure 2. Scalars describing satellite shape around the LG galaxies for a fixed number of satellites N_s=11: plane width w in physical units, c/a ratio and b/a ratio. Left: M31, right: MW. The square at the center are observations; the 2D histograms are the contour levels after randomizing 10^4 the satellite positions while keeping the radial distribution fixed; the blue circles are the results from Illustris-1-Dark. For the M31 these three results (observations, randomized observations and simulations) seem to be in broad agreement, while for the MW the three results clearly differ. The corresponding plots for Illustris-1 and ELVIS are in Figures C1 and C2, respectively.
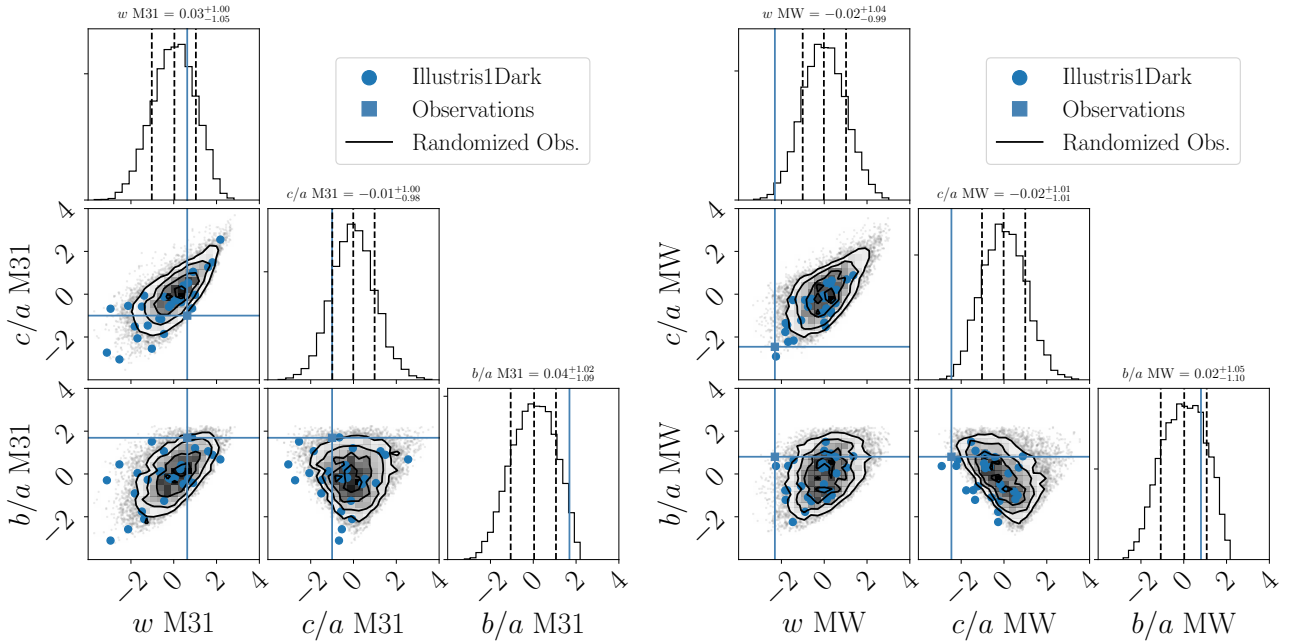

Figure 3. Same layout as Figure 2. Each scalar quantity is re-centered and normalized by the mean value and standard deviation from the 10^4 randomizations. The distribution from the randomizations (plots over the diagonal) now has by definition a mean of zero and standard deviation of one. The results for the width and c/a ratio of MW satellites are more than two standard deviations away from the mean. The corresponding plots for Illustris-1 and ELVIS are in Figures C1 and C2, respectively.
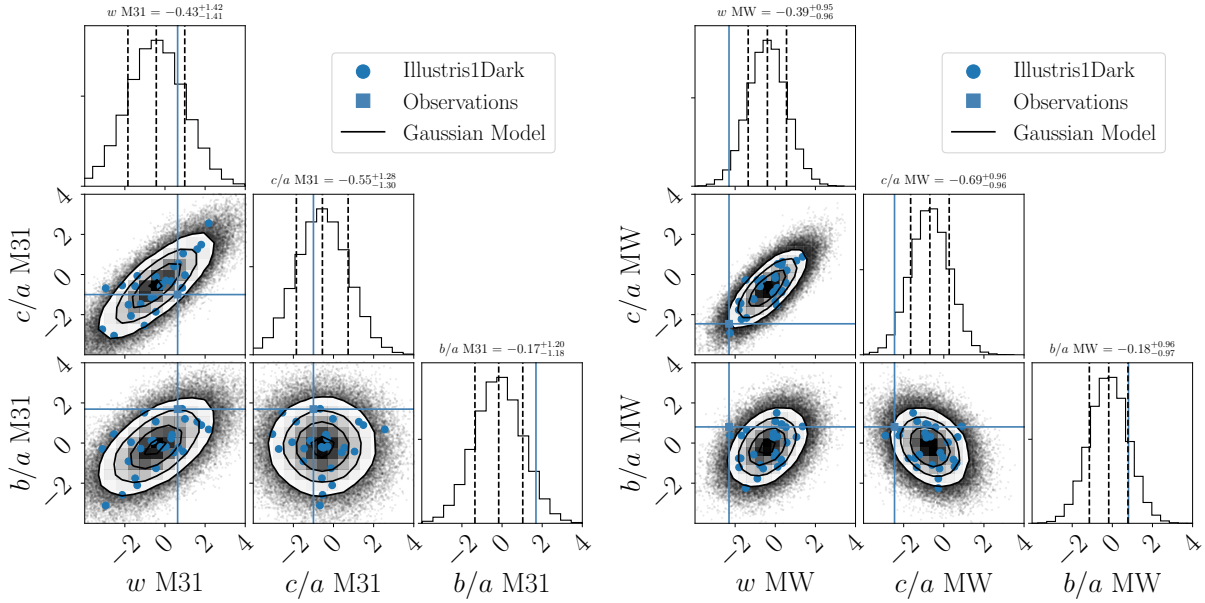
Figure 4. Same layout as Figure 3. This time the distribution comes from the multivariate gaussian model with its parameters estimated from the Illustris-1-Dark results. The corresponding plots for Illustris-1 and ELVIS are in Figures C1 and C2, respectively.

two simulations are included in the Appendix C. The full covariance matrices are in the Appendix B.

4.1 Physical Units

Figure 2 summarizes the results in physical units. It compares three different groups: observations, simulations and the observations randomized. The left panel shows the results for M31 and the panel on the left for the MW.

The most interesting outcome is that the MW plane width is smaller than $\approx 98\%$ of the planes computed from the randomized distribution; its c/a ratio is also significantly lower than the measured values for the randomized distributions. On the other hand the results for $M31$ for the same quantities are within 1σ of the randomized results.

The comparison against observations also provides an extreme picture for the MW. In this case the mean witdh from simulation is almost twice as the mean width from the randomization. A possible criticism to this result is that the typical halo mass in the simulation is larger than the it is for the MW. For this reason we renormalize all quantities (w, c/a and b/a) to the mean value and standard deviation provided by its spherical randomization. In this way the physical scale of the halo becomes a second order effect and only the deviations from asphericity are protagonist.

4.2 Normalized Units

Figure 3 summarizes the results of renormalizing to the randomized results. The layout is the same as Figure 2. By construction, the relative position of the observations and the randomized results keeps constant; The MW continues to be atypical with respect to its own randomized distribution.

The most notorious difference comes from the changes in the simulations. The previous large difference between the width distribution from MW observations and simulations

is reduced. The reason is that normalized quantities are not dependent on the physical scale anymore; only the deviations from asphericity are important.

The distributions for the normalized quantities from simulations are well described by gaussians. The parameters of the gaussian model (covariance matrix and mean) are different depending on the simulation and number of particles, but all of them are well described by the multivariate gaussian.

4.3 Multivariate Gaussian model

Figure 4 summarized the results from computing the covariance matrix and mean vector in Eq.2 from the normalized quantities obtained from the Illustris-1-Dark simulation. The distributions in this Figure are computed from 10^6 points generated with the multivariate gaussian.

This nicely summarizes the results we had in the previous sections. The left hand triangular plot shows how M31 falls within the 2σ contours in the 2D scatter plots; while the right hand plot clearly places the MW observations at the border of the 3σ range in the joint distributions that involve the width w.

In both cases the strongest positive correlation is present for the width and the c/a axis ratio. A weaker correlation is present for the width and the b/a axis ratio. The weakest correlation, positive or negative depending on the simulation, is present for the c/a ratio and b/a ratio.

The mean values also hold valuable information. For the three quantities the mean is negative, a quantification trend that the satellite distribution from LCDM simulations tend to be aspherical. This trend has a very few exceptions. Nmely the ELVIS results for M31 with $N_s = 11, 12$ and the Illustris-1 results for the MW with $N_s = 11$, which are consistent with an spherical distribution. We also computed

the correlation between the M31 and MW results, finding that it is very weak and can be safely discarded.

The explicity formulation for this probability distribution allows us to generate large samples with asphericity properties consistent with the parent simulation. From this samples we can explicitly compute the fraction of systems that, for instance, show the extreme MW values.

4.4 Number of Expected LG Systems

Using the multivariate gaussian model we generate 10^3 samples, each sample containing 10^4 pairs, where each pair member is drawn from the corresponding multivariate gaussian distribution.

We consider that a sampled system is similar to the M31/MW galaxy if the absolute distance of each of its normalized characteristics (w, c/a, b/a) to the sample mean is equal or larger than the absolute distance of the observational values to the sample mean. That is, we perform a double-tailed test around the mean using the observational values as a threshold.

Figure 5 summarizes the results from this experiment as a function of satellite number for all three simulations: Illustris-1-Dark, Illustris-1 and ELVIS.

Considering the joint distribution of M31 and MW we find that at most 2% of the pairs are expected to be similar to the LG. In a three dimensional gaussian distribution, having a 1σ, 2σ and 3σ interval corresponds to having respectively 19%, 73% and 97% of the total of points in the distribution. With this result in mind the LG has the same degree of atypicality as a 3σ outlier.

For M31, between 5% and 80% of the pairs have a satellite distribution as aspherical as the one observed in M31. This fraction drops dramatically for the MW where only 0.02% to 4% of the satellites are expected to have as extreme aspherical distributions as the MW. A consistent finding is that the M31 fraction is always larger than the MW fraction at fixed N_s and simulation.

Among the three simulations, the results inferred from ELVIS data show the lowest fraction of M31 and MW systems; for Illustris-1-Dark we have the highest fraction of M31/MW systems. The results from Illustris-1 are in between these two simulations, but closer to ELVIS.

A probable reason for these trends is the different median mass for the MW/M31 halos in the pairs from these simulations. For instance for the MW halo the median maximum circular velocity is ~ 160 km s^{-1}, ~ 150 km s^{-1} and ~ 120 km s^{-1} in the ELVIS, Illustris-1 and Illustris-1-Dark simulations, respectively. For the M31 halo this median velocity is ~ 200km s^{-1} both for the ELVIS and Illustris1 simulations, while for the Illustris-1-Dark it is ~ 160 km s^{-1}.

Another element that influences this trend is the simulated physics. This is evident in the comparison between Illustris-1 and Illustris-1-Dark. These two simulations share the same characteristics except for the inclusion of baryonic physics in Illustris-1. We find that extreme MW systems are easier to find in the DM only simulation. The results listed in Appendix B show that halos are closer to spherical once baryonic effects are included. For instance for $N_p = 11$ the mean value for the normalized width goes closer to zero, from -0.43 ± 0.04 to -0.03 ± 0.06, and the same is true for the c/a ratio that changes from -0.56 ± 0.06 in the DM

only simulation to -0.24 ± 0.06 in Illustris-1. This trend has been reported before for the DM distribution in the whole halo Bryan et al. (2013). Our results suggest that it also hold for the satellite distribution. We postpone a detailed quantification of this effect for a future study.

4.5 How to understand an atypical MW

The highly aspherical satellite distribution in the MW is another piece of information that points at an atypical configuration in LCDM. We also have the number of satellites as bright as the Magellanic Clouds, only expected in 5% of galaxies (Busha et al. 2011) and the satellite velocities around the MW with a radial/tangential anisotropy only expected in 3% of systems in LCDM (Cautun & Frenk 2017). One could also add the atypical kinematics of M31 with a very low tangential velocity, which is only expected in less than 1% of the pairs with similar environmental characteristics (Forero-Romero et al. 2013). With the small numbers that we have in the simulations we used we cannot study properly those correlations. We cannot even find a clear trend linking asphericity to halo mass or another pair property.

Assuming that these atypical properties are independent one would need at least 10^6 pairs in order to find a single pair that meets all four characteristics (aspherical satellite distribution, bright Magellanic Clouds, satellite velocity anisotropy and atypical pair kinematics). Using the number density for pairs in Illustris-1 (2×10^{-5} pairs/Mpc^3) this would imply a cubic simulation volume of 5 Gpc on a side, something unfeasible under current technology. However, studying two characteristics at a time to find possible correlations, and at least one pair resembling observations, reduces the box size to 500 Mpc, something that is close to current simulations such as Illustris-TNG (Pillepich et al. 2018).

5 CONCLUSIONS

In this paper we developed and demonstrated a method to quantify the asphericity of the satellite distribution around the MW and M31. In the interest of keeping the demonstration straightforward and robust we focus on the asphericity estimates for a fixed number of the brightest satellites around each galaxy.

The method uses as a reference the spherically randomized data of the system under study (Pawlowski et al. 2017). To this end, we first measure the width and axis ratios for the satellite distributions of interest. Then, we measure the same quantities for the same set of points after the spherical randomization process. Finally, we renormalize the initial results to the mean value and standard deviation computed from the randomized data.

We found that these normalized quantities are well described by a multivariate gaussian distribution We estimated the mean and covariance of these distributions using the results of LG pairs coming from three different numerical simulations (Illustris-1, Illustris-1-Dark and ELVIS). Finally, we compared the observational results against the distributions derived from the simulations
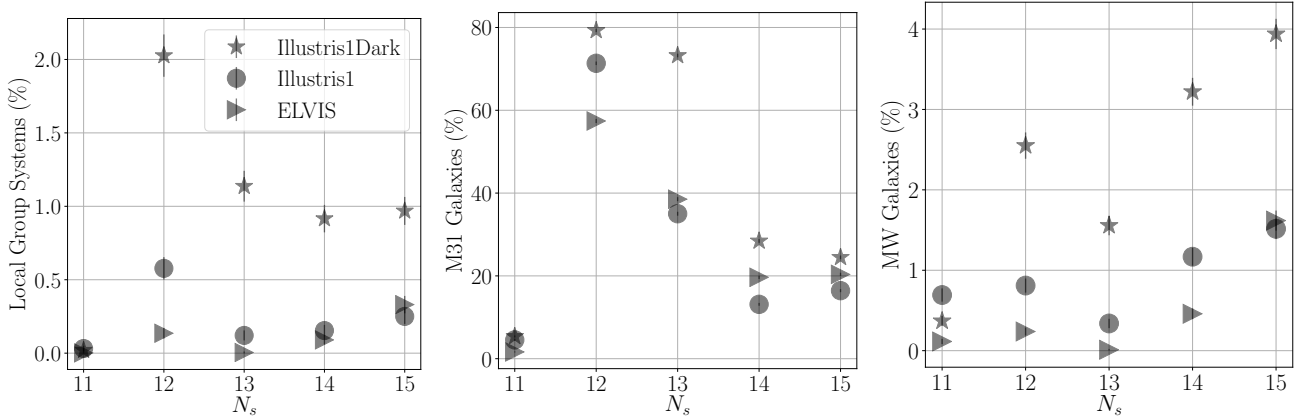
We quantified that in the best case (Illustris-1-Dark)

Figure 5. Percentage of systems that have asphericity scalars as extreme as the LG (left), M31 (middle) and MW (right). This percentage is computed as a function of satellite number for all the three simulations (Illustris-1-Dark, Illustris-1 and ELVIS). The common trend is that at most of 2% of LG-like pairs are expected to be as extreme as observations, with most of the weight of this atypicality falls onto the MW; at most 4% of similar systems have such an aspherical satellite distribution.

the degree of asphericity in the observed LG is only expected in 2% of the pairs. This places the LG as a 3σ outlier. The weight to explain this atypical result is not distributed equally between the MW and M31. While M31 presents a fully typical asphericity in the expectations from LCDM, the MW shows aspherical deviations in plane width and the major-to-minor axis ratio highly atypical in the framework of LCDM, confirming the original hint by Kroupa et al. (2005) and more recent results by Pawlowski et al. (2015). We estimated that with the M31 between 5% and 80% of the pairs show aspherical characteristics larger than M31, while this fraction drops to less than 4% for the MW. These fractions are robust to changes in the numerical simulations, the criteria used to define the pairs, the way to select the satellites and to the methods used to estimate the parameters of the multivariate normal distribution.

The focus of our approach was building an explicit probability distribution for the observables of interest, instead of trying to find simulated objects that fulfill different observational criteria. This approach is particularly useful in the case of atypical observables, as it allows for an atypicality quantification without building explicit samples of objects that are already scarce and difficult to find in simulations.

An extension of this framework to outliers in higher order deviations (i.e. coherent *velocity* structures) should also be possible, provided that an explicit probability distribution for the scalars of interest can be built. The approach presented here is also useful to gauge the influence of influence of different physical elements includes the simulation. For instance, in our case the data hints towards rounder satellite distributions in simulations that include baryonic effects.

This atypicality should be seen as an opportunity to constrain in great detail the environment that allowed such a pattern to emerge. Although broad correlations between LG assembly, pair kinematics, halo shapes and satellite distributions are expected in LCDM (Forero-Romero et al. 2011, 2014; Forero-Romero & González 2015; Libeskind et al. 2015), we claim that detailed studies of the satellite asphericity as a function of halo mass and cosmic web environment are still missing to understand what features in the initial

conditions of our LG are responsible for the extreme features observed in its satellite distribution.

REFERENCES

Ahmed S. H., Brooks A. M., Christensen C. R., 2017, MNRAS, 466, 3119

Boylan-Kolchin M., Bullock J. S., Kaplinghat M., 2011, MNRAS, 415, L40

Bryan S. E., Kay S. T., Duffy A. R., Schaye J., Dalla Vecchia C., Booth C. M., 2013, MNRAS, 429, 3316

Buck T., Macciò A. V., Dutton A. A., 2015, ApJ, 809, 49

Buck T., Dutton A. A., Macciò A. V., 2016, MNRAS, 460, 4348

Busha M. T., Wechsler R. H., Behroozi P. S., Gerke B. F., Klypin A. A., Primack J. R., 2011, ApJ, 743, 117

Cautun M., Frenk C. S., 2017, MNRAS, 468, L41

Cautun M., Bose S., Frenk C. S., Guo Q., Han J., Hellwing W. A., Sawala T., Wang W., 2015, MNRAS, 452, 3838

Collins M. L. M., et al., 2015, ApJ, 799, L13

Conn A. R., et al., 2013, ApJ, 766, 120

Conroy C., Wechsler R. H., Kravtsov A. V., 2006, ApJ, 647, 201

Fernando N., Arias V., Guglielmo M., Lewis G. F., Ibata R. A., Power C., 2017, MNRAS, 465, 641

Forero-Romero J. E., González R., 2015, ApJ, 799, 45

Forero-Romero J. E., Hoffman Y., Yepes G., Gottlöber S., Piontek R., Klypin A., Steinmetz M., 2011, MNRAS, 417, 1434

Forero-Romero J. E., Hoffman Y., Bustamante S., Gottlöber S., Yepes G., 2013, ApJ, 767, L5

Forero-Romero J. E., Contreras S., Padilla N., 2014, MNRAS, 443, 1090

Garrison-Kimmel S., Boylan-Kolchin M., Bullock J. S., Lee K., 2014, MNRAS, 438, 2578

Gillet N., Ocvirk P., Aubert D., Knebe A., Libeskind N., Yepes G., Gottlöber S., Hoffman Y., 2015, ApJ, 800, 34

Guo Q., White S., Li C., Boylan-Kolchin M., 2010, MNRAS, 404, 1111

Hinshaw G., et al., 2013, ApJS, 208, 19

Ibata R. A., et al., 2013, Nature, 493, 62

Koch A., Grebel E. K., 2006, AJ, 131, 1405

Kravtsov A. V., Berlind A. A., Wechsler R. H., Klypin A. A., Gottlöber S., Allgood B., Primack J. R., 2004, ApJ, 609, 35

Kroupa P., Theis C., Boily C. M., 2005, A&A, 431, 517

Kunkel W. E., Demers S., 1976, in Dickens R. J., Perry J. E., Smith F. G., King I. R., eds, Royal Greenwich Observatory Bulletins Vol. 182, The Galaxy and the Local Group. p. 241

Libeskind N. I., Frenk C. S., Cole S., Helly J. C., Jenkins A., Navarro J. F., Power C., 2005, MNRAS, 363, 146

Libeskind N. I., Frenk C. S., Cole S., Jenkins A., Helly J. C., 2009, MNRAS, 399, 550

Libeskind N. I., Hoffman Y., Tully R. B., Courtois H. M., Pomarède D., Gottlöber S., Steinmetz M., 2015, MNRAS, 452, 1052

Lynden-Bell D., 1976, MNRAS, 174, 695

McConnachie A. W., 2012, AJ, 144, 4

Metz M., Kroupa P., Jerjen H., 2007, MNRAS, 374, 1125

Pawlowski M. S., McGaugh S. S., 2014, ApJ, 789, L24

Pawlowski M. S., Kroupa P., Jerjen H., 2013, MNRAS, 435, 1928

Pawlowski M. S., Kroupa P., Jerjen H., 2014, VizieR Online Data Catalog, 743

Pawlowski M. S., Famaey B., Merritt D., Kroupa P., 2015, ApJ, 815, 19

Pawlowski M. S., et al., 2017, Astronomische Nachrichten, 338, 854

Pillepich A., et al., 2018, MNRAS, 473, 4077

Sawala T., et al., 2016, MNRAS, 457, 1931

Springel V., 2010, MNRAS, 401, 791

Starkenburg E., et al., 2013, MNRAS, 429, 725

Vogelsberger M., et al., 2014, MNRAS, 444, 1518

Wang J., Frenk C. S., Cooper A. P., 2013, MNRAS, 429, 1502

Zentner A. R., Kravtsov A. V., Gnedin O. Y., Klypin A. A., 2005, ApJ, 629, 219

APPENDIX A: PHYSICAL CHARACTERISTICS OF THE ISOLATED PAIRS SAMPLES

APPENDIX B: COVARIANCE MATRICES AND MEAN VALUE VECTORS

B1   Illustris-1-Dark, M31, $N_s = 11$

$$\Sigma = \begin{bmatrix} 2.02 \pm 0.09 & 1.46 \pm 0.09 & 0.97 \pm 0.07 \\ 1.46 \pm 0.09 & 1.69 \pm 0.10 & -0.01 \pm 0.05 \\ 0.97 \pm 0.07 & -0.01 \pm 0.05 & 1.42 \pm 0.08 \end{bmatrix}$$

$$\mu = \begin{bmatrix} -0.43 \pm 0.06 & -0.56 \pm 0.06 & -0.17 \pm 0.05 \end{bmatrix}$$

B2   Illustris-1-Dark, MW, $N_s = 11$

$$\Sigma = \begin{bmatrix} 0.94 \pm 0.04 & 0.71 \pm 0.04 & 0.36 \pm 0.03 \\ 0.71 \pm 0.04 & 0.93 \pm 0.05 & -0.27 \pm 0.03 \\ 0.36 \pm 0.03 & -0.27 \pm 0.03 & 0.94 \pm 0.04 \end{bmatrix}$$

$$\mu = \begin{bmatrix} -0.40 \pm 0.04 & -0.69 \pm 0.04 & -0.19 \pm 0.04 \end{bmatrix}$$
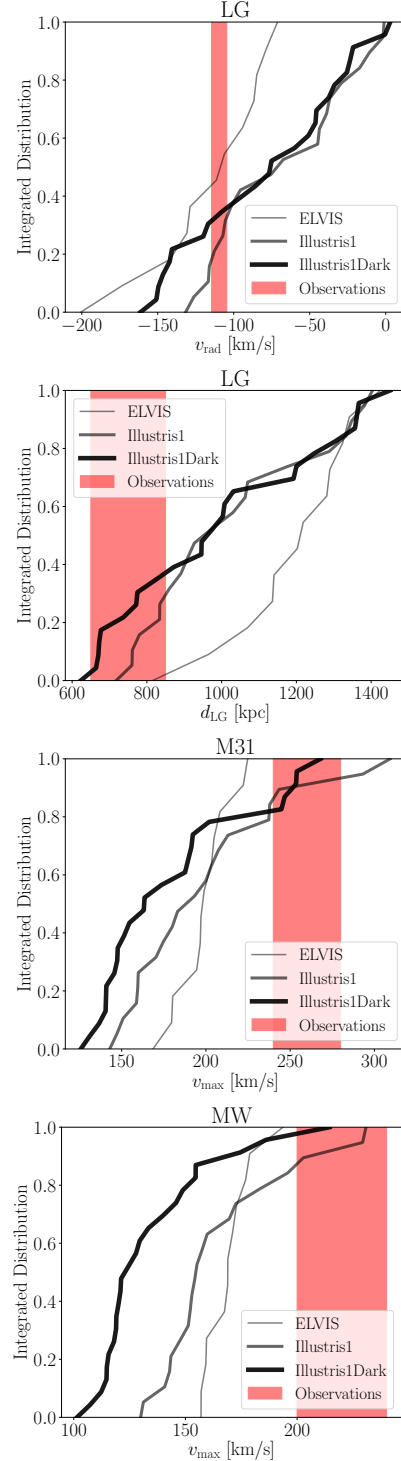

Figure A1. Physical characteristics of the LG pairs selected in the simulations. All plots show the integrated distributions. The physical properties are the radial comoving velocity between the MW and M31, the radial separation between the MW and M31 and the maximum circular velocity for the M31 and MW dark matter halo.

B3   Illustris-1, M31, $N_s = 11$

$$\Sigma = \begin{bmatrix} 1.59 \pm 0.08 & 1.23 \pm 0.07 & 0.80 \pm 0.06 \\ 1.23 \pm 0.07 & 1.44 \pm 0.08 & 0.01 \pm 0.06 \\ 0.80 \pm 0.06 & 0.01 \pm 0.06 & 1.26 \pm 0.08 \end{bmatrix}$$

$$\mu = \begin{bmatrix} 0.03 \pm 0.06 & -0.24 \pm 0.06 & -0.01 \pm 0.05 \end{bmatrix}$$

B4   Illustris-1, MW, $N_s = 11$

$$\Sigma = \begin{bmatrix} 1.01 \pm 0.05 & 0.72 \pm 0.05 & 0.62 \pm 0.04 \\ 0.72 \pm 0.05 & 0.78 \pm 0.05 & 0.12 \pm 0.03 \\ 0.62 \pm 0.04 & 0.12 \pm 0.03 & 0.80 \pm 0.04 \end{bmatrix}$$

$$\mu = \begin{bmatrix} -0.07 \pm 0.05 & -0.45 \pm 0.04 & 0.02 \pm 0.04 \end{bmatrix}$$

B5   ELVIS, M31, $N_s = 11$

$$\Sigma = \begin{bmatrix} 1.77 \pm 0.23 & 1.44 \pm 0.18 & 0.65 \pm 0.09 \\ 1.44 \pm 0.18 & 1.54 \pm 0.15 & 0.15 \pm 0.06 \\ 0.65 \pm 0.09 & 0.15 \pm 0.06 & 0.77 \pm 0.11 \end{bmatrix}$$

$$\mu = \begin{bmatrix} 0.07 \pm 0.09 & -0.06 \pm 0.08 & -0.08 \pm 0.06 \end{bmatrix}$$

B6   ELVIS, MW, $N_s = 11$

$$\Sigma = \begin{bmatrix} 0.59 \pm 0.06 & 0.61 \pm 0.11 & 0.11 \pm 0.08 \\ 0.61 \pm 0.11 & 1.25 \pm 0.19 & -0.71 \pm 0.12 \\ 0.11 \pm 0.08 & -0.71 \pm 0.12 & 1.13 \pm 0.11 \end{bmatrix}$$

$$\mu = \begin{bmatrix} -0.25 \pm 0.05 & -0.59 \pm 0.08 & -0.16 \pm 0.07 \end{bmatrix}$$

B7   Illustris-1-Dark, M31, $N_s = 12$

$$\Sigma = \begin{bmatrix} 2.34 \pm 0.11 & 1.72 \pm 0.11 & 1.10 \pm 0.06 \\ 1.72 \pm 0.11 & 1.72 \pm 0.11 & 0.35 \pm 0.05 \\ 1.10 \pm 0.06 & 0.35 \pm 0.05 & 1.21 \pm 0.07 \end{bmatrix}$$

$$\mu = \begin{bmatrix} -0.58 \pm 0.07 & -0.49 \pm 0.06 & -0.41 \pm 0.05 \end{bmatrix}$$

B8   Illustris-1-Dark, MW, $N_s = 12$

$$\Sigma = \begin{bmatrix} 1.25 \pm 0.06 & 0.97 \pm 0.06 & 0.62 \pm 0.04 \\ 0.97 \pm 0.06 & 1.19 \pm 0.06 & -0.11 \pm 0.05 \\ 0.62 \pm 0.04 & -0.11 \pm 0.05 & 1.19 \pm 0.04 \end{bmatrix}$$

$$\mu = \begin{bmatrix} -0.38 \pm 0.05 & -0.55 \pm 0.05 & -0.28 \pm 0.05 \end{bmatrix}$$

B9   Illustris-1, M31, $N_s = 12$

$$\Sigma = \begin{bmatrix} 1.01 \pm 0.06 & 0.74 \pm 0.04 & 0.59 \pm 0.06 \\ 0.74 \pm 0.04 & 1.03 \pm 0.05 & -0.16 \pm 0.04 \\ 0.59 \pm 0.06 & -0.16 \pm 0.04 & 1.12 \pm 0.06 \end{bmatrix}$$

$$\mu = \begin{bmatrix} -0.09 \pm 0.05 & -0.23 \pm 0.05 & -0.33 \pm 0.05 \end{bmatrix}$$

B10   Illustris-1, MW, $N_s = 12$

$$\Sigma = \begin{bmatrix} 1.00 \pm 0.05 & 0.69 \pm 0.05 & 0.64 \pm 0.05 \\ 0.69 \pm 0.05 & 0.87 \pm 0.06 & -0.06 \pm 0.04 \\ 0.64 \pm 0.05 & -0.06 \pm 0.04 & 1.06 \pm 0.06 \end{bmatrix}$$

$$\mu = \begin{bmatrix} -0.16 \pm 0.05 & -0.46 \pm 0.04 & -0.12 \pm 0.05 \end{bmatrix}$$

B11   ELVIS, M31, $N_s = 12$

$$\Sigma = \begin{bmatrix} 1.97 \pm 0.28 & 1.64 \pm 0.21 & 0.57 \pm 0.11 \\ 1.64 \pm 0.21 & 1.69 \pm 0.17 & 0.11 \pm 0.07 \\ 0.57 \pm 0.11 & 0.11 \pm 0.07 & 0.70 \pm 0.12 \end{bmatrix}$$

$$\mu = \begin{bmatrix} -0.06 \pm 0.09 & -0.18 \pm 0.09 & -0.13 \pm 0.06 \end{bmatrix}$$

B12   ELVIS, MW, $N_s = 12$

$$\Sigma = \begin{bmatrix} 0.58 \pm 0.05 & 0.47 \pm 0.10 & 0.23 \pm 0.09 \\ 0.47 \pm 0.10 & 1.04 \pm 0.16 & -0.68 \pm 0.09 \\ 0.23 \pm 0.09 & -0.68 \pm 0.09 & 1.23 \pm 0.11 \end{bmatrix}$$

$$\mu = \begin{bmatrix} -0.42 \pm 0.05 & -0.78 \pm 0.07 & -0.16 \pm 0.07 \end{bmatrix}$$

B13   Illustris-1-Dark, M31, $N_s = 13$

$$\Sigma = \begin{bmatrix} 1.79 \pm 0.09 & 1.19 \pm 0.08 & 0.90 \pm 0.06 \\ 1.19 \pm 0.08 & 1.12 \pm 0.07 & 0.17 \pm 0.03 \\ 0.90 \pm 0.06 & 0.17 \pm 0.03 & 1.12 \pm 0.07 \end{bmatrix}$$

$$\mu = \begin{bmatrix} -0.61 \pm 0.06 & -0.67 \pm 0.05 & -0.37 \pm 0.05 \end{bmatrix}$$

B14   Illustris-1-Dark, MW, $N_s = 13$

$$\Sigma = \begin{bmatrix} 1.30 \pm 0.07 & 1.09 \pm 0.06 & 0.52 \pm 0.05 \\ 1.09 \pm 0.06 & 1.42 \pm 0.08 & -0.18 \pm 0.06 \\ 0.52 \pm 0.05 & -0.18 \pm 0.06 & 1.09 \pm 0.04 \end{bmatrix}$$

$$\mu = \begin{bmatrix} -0.38 \pm 0.05 & -0.54 \pm 0.05 & -0.30 \pm 0.05 \end{bmatrix}$$

B15   Illustris-1, M31, $N_s = 13$

$$\Sigma = \begin{bmatrix} 1.36 \pm 0.09 & 0.89 \pm 0.05 & 0.97 \pm 0.06 \\ 0.89 \pm 0.05 & 0.92 \pm 0.05 & 0.22 \pm 0.05 \\ 0.97 \pm 0.06 & 0.22 \pm 0.05 & 1.28 \pm 0.06 \end{bmatrix}$$

$$\mu = \begin{bmatrix} -0.07 \pm 0.06 & -0.17 \pm 0.05 & -0.30 \pm 0.06 \end{bmatrix}$$

B16   Illustris-1, MW, $N_s = 13$

$$\Sigma = \begin{bmatrix} 0.95 \pm 0.08 & 0.90 \pm 0.09 & 0.33 \pm 0.05 \\ 0.90 \pm 0.09 & 1.29 \pm 0.10 & -0.24 \pm 0.05 \\ 0.33 \pm 0.05 & -0.24 \pm 0.05 & 0.89 \pm 0.08 \end{bmatrix}$$

$$\mu = \begin{bmatrix} -0.13 \pm 0.05 & -0.47 \pm 0.06 & -0.09 \pm 0.05 \end{bmatrix}$$

B17   ELVIS, M31, $N_s = 13$

$$\Sigma = \begin{bmatrix} 1.99 \pm 0.22 & 1.49 \pm 0.19 & 0.98 \pm 0.11 \\ 1.49 \pm 0.19 & 1.45 \pm 0.15 & 0.38 \pm 0.10 \\ 0.98 \pm 0.11 & 0.38 \pm 0.10 & 1.06 \pm 0.17 \end{bmatrix}$$

$$\mu = \begin{bmatrix} -0.18 \pm 0.10 & -0.37 \pm 0.08 & -0.07 \pm 0.07 \end{bmatrix}$$

B18   ELVIS, MW, $N_s = 13$

$$\Sigma = \begin{bmatrix} 0.43 \pm 0.05 & 0.54 \pm 0.09 & -0.12 \pm 0.07 \\ 0.54 \pm 0.09 & 1.20 \pm 0.17 & -0.85 \pm 0.12 \\ -0.12 \pm 0.07 & -0.85 \pm 0.12 & 0.94 \pm 0.10 \end{bmatrix}$$

$$\mu = \begin{bmatrix} -0.44 \pm 0.04 & -0.73 \pm 0.07 & -0.30 \pm 0.07 \end{bmatrix}$$

B19   Illustris-1-Dark, M31, $N_s = 14$

$$\Sigma = \begin{bmatrix} 1.60 \pm 0.11 & 1.34 \pm 0.09 & 0.68 \pm 0.05 \\ 1.34 \pm 0.09 & 1.32 \pm 0.08 & 0.28 \pm 0.04 \\ 0.68 \pm 0.05 & 0.28 \pm 0.04 & 0.85 \pm 0.05 \end{bmatrix}$$

$$\mu = \begin{bmatrix} -0.33 \pm 0.06 & -0.53 \pm 0.05 & -0.15 \pm 0.04 \end{bmatrix}$$

B20   Illustris-1-Dark, MW, $N_s = 14$

$$\Sigma = \begin{bmatrix} 1.27 \pm 0.06 & 1.12 \pm 0.06 & 0.40 \pm 0.04 \\ 1.12 \pm 0.06 & 1.55 \pm 0.08 & -0.32 \pm 0.05 \\ 0.40 \pm 0.04 & -0.32 \pm 0.05 & 1.02 \pm 0.04 \end{bmatrix}$$

$$\mu = \begin{bmatrix} -0.52 \pm 0.05 & -0.64 \pm 0.06 & -0.40 \pm 0.05 \end{bmatrix}$$

B21   Illustris-1, M31, $N_s = 14$

$$\Sigma = \begin{bmatrix} 1.11 \pm 0.05 & 0.88 \pm 0.05 & 0.83 \pm 0.05 \\ 0.88 \pm 0.05 & 1.14 \pm 0.06 & 0.08 \pm 0.05 \\ 0.83 \pm 0.05 & 0.08 \pm 0.05 & 1.39 \pm 0.07 \end{bmatrix}$$

$$\mu = \begin{bmatrix} -0.06 \pm 0.05 & -0.24 \pm 0.05 & -0.23 \pm 0.06 \end{bmatrix}$$

B22   Illustris-1, MW, $N_s = 14$

$$\Sigma = \begin{bmatrix} 0.99 \pm 0.07 & 0.88 \pm 0.08 & 0.38 \pm 0.06 \\ 0.88 \pm 0.08 & 1.24 \pm 0.10 & -0.26 \pm 0.07 \\ 0.38 \pm 0.06 & -0.26 \pm 0.07 & 0.97 \pm 0.09 \end{bmatrix}$$

$$\mu = \begin{bmatrix} -0.39 \pm 0.05 & -0.62 \pm 0.06 & -0.28 \pm 0.05 \end{bmatrix}$$

B23   ELVIS, M31, $N_s = 14$

$$\Sigma = \begin{bmatrix} 2.04 \pm 0.24 & 1.21 \pm 0.14 & 1.27 \pm 0.17 \\ 1.21 \pm 0.14 & 0.97 \pm 0.09 & 0.45 \pm 0.09 \\ 1.27 \pm 0.17 & 0.45 \pm 0.09 & 1.31 \pm 0.19 \end{bmatrix}$$

$$\mu = \begin{bmatrix} -0.37 \pm 0.10 & -0.38 \pm 0.07 & -0.40 \pm 0.08 \end{bmatrix}$$

B24   ELVIS, MW, $N_s = 14$

$$\Sigma = \begin{bmatrix} 0.82 \pm 0.08 & 1.06 \pm 0.14 & -0.11 \pm 0.06 \\ 1.06 \pm 0.14 & 1.75 \pm 0.20 & -0.62 \pm 0.09 \\ -0.11 \pm 0.06 & -0.62 \pm 0.09 & 0.64 \pm 0.07 \end{bmatrix}$$

$$\mu = \begin{bmatrix} -0.38 \pm 0.06 & -0.74 \pm 0.09 & -0.13 \pm 0.05 \end{bmatrix}$$

B25   Illustris-1-Dark, M31, $N_s = 15$

$$\Sigma = \begin{bmatrix} 1.65 \pm 0.10 & 1.35 \pm 0.09 & 0.81 \pm 0.06 \\ 1.35 \pm 0.09 & 1.34 \pm 0.09 & 0.36 \pm 0.05 \\ 0.81 \pm 0.06 & 0.36 \pm 0.05 & 0.97 \pm 0.05 \end{bmatrix}$$

$$\mu = \begin{bmatrix} -0.31 \pm 0.06 & -0.51 \pm 0.05 & -0.16 \pm 0.05 \end{bmatrix}$$

B26   Illustris-1-Dark, MW, $N_s = 15$

$$\Sigma = \begin{bmatrix} 1.52 \pm 0.07 & 1.25 \pm 0.06 & 0.64 \pm 0.05 \\ 1.25 \pm 0.06 & 1.58 \pm 0.08 & -0.15 \pm 0.06 \\ 0.64 \pm 0.05 & -0.15 \pm 0.06 & 1.18 \pm 0.05 \end{bmatrix}$$

$$\mu = \begin{bmatrix} -0.50 \pm 0.06 & -0.63 \pm 0.06 & -0.33 \pm 0.05 \end{bmatrix}$$

B27   Illustris-1, M31, $N_s = 15$

$$\Sigma = \begin{bmatrix} 1.18 \pm 0.04 & 0.91 \pm 0.05 & 0.84 \pm 0.05 \\ 0.91 \pm 0.05 & 1.11 \pm 0.07 & 0.15 \pm 0.04 \\ 0.84 \pm 0.05 & 0.15 \pm 0.04 & 1.23 \pm 0.06 \end{bmatrix}$$

$$\mu = \begin{bmatrix} -0.25 \pm 0.06 & -0.41 \pm 0.05 & -0.32 \pm 0.06 \end{bmatrix}$$

B28   Illustris-1, MW, $N_s = 15$

$$\Sigma = \begin{bmatrix} 1.06 \pm 0.07 & 0.88 \pm 0.07 & 0.44 \pm 0.06 \\ 0.88 \pm 0.07 & 1.11 \pm 0.08 & -0.11 \pm 0.05 \\ 0.44 \pm 0.06 & -0.11 \pm 0.05 & 0.84 \pm 0.08 \end{bmatrix}$$

$$\mu = \begin{bmatrix} -0.45 \pm 0.05 & -0.67 \pm 0.05 & -0.32 \pm 0.05 \end{bmatrix}$$

B29   ELVIS, M31, $N_s = 15$

$$\Sigma = \begin{bmatrix} 1.51 \pm 0.13 & 1.16 \pm 0.11 & 0.74 \pm 0.11 \\ 1.16 \pm 0.11 & 1.06 \pm 0.11 & 0.32 \pm 0.06 \\ 0.74 \pm 0.11 & 0.32 \pm 0.06 & 0.75 \pm 0.10 \end{bmatrix}$$

$$\mu = \begin{bmatrix} -0.41 \pm 0.08 & -0.47 \pm 0.07 & -0.48 \pm 0.06 \end{bmatrix}$$

B30   ELVIS, MW, $N_s = 15$

$$\Sigma = \begin{bmatrix} 1.13 \pm 0.15 & 1.42 \pm 0.20 & -0.06 \pm 0.08 \\ 1.42 \pm 0.20 & 2.16 \pm 0.25 & -0.58 \pm 0.09 \\ -0.06 \pm 0.08 & -0.58 \pm 0.09 & 0.74 \pm 0.09 \end{bmatrix}$$

$$\mu = \begin{bmatrix} -0.47 \pm 0.07 & -0.72 \pm 0.10 & -0.26 \pm 0.06 \end{bmatrix}$$

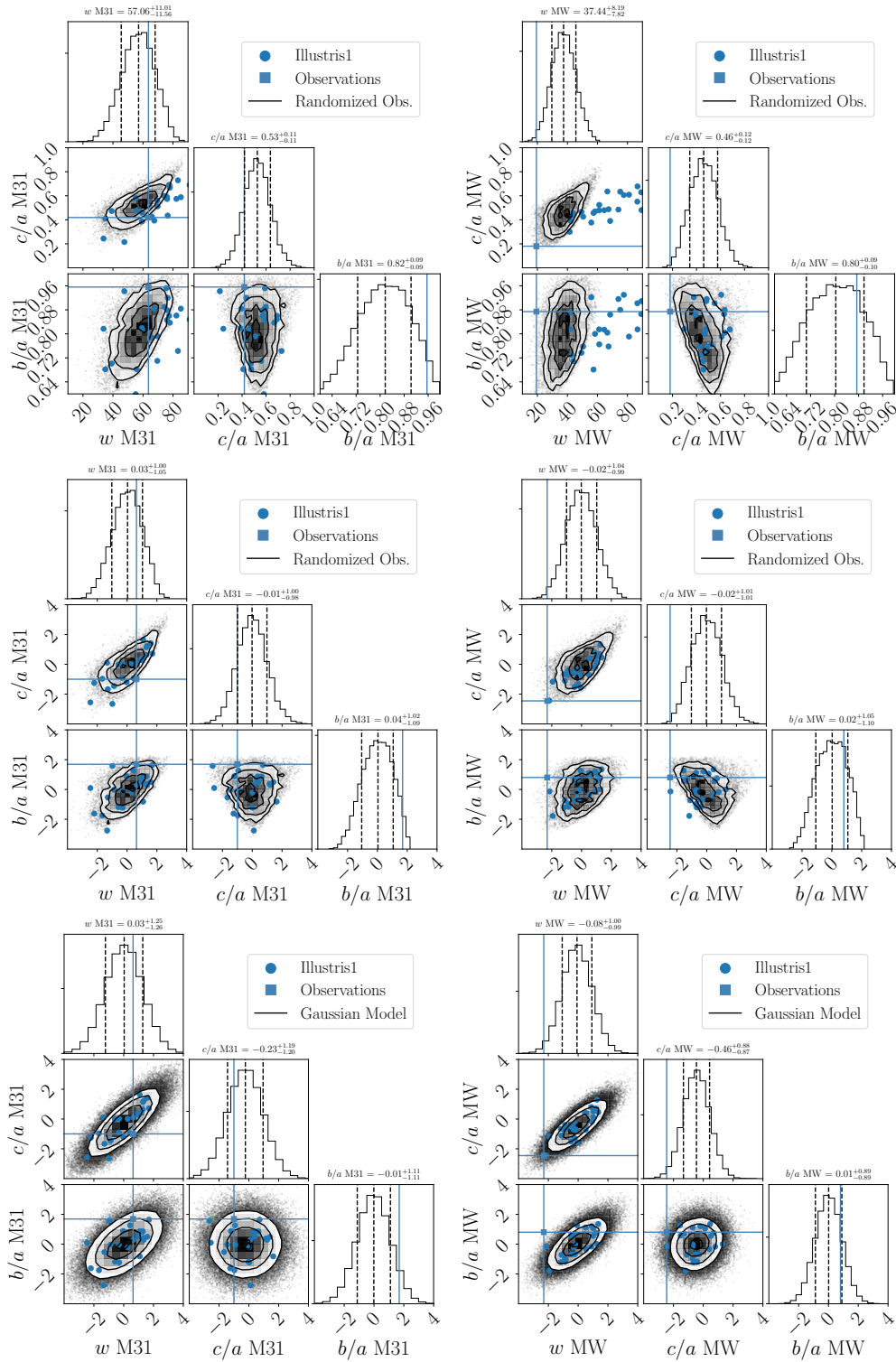# APPENDIX C: RESULTS FROM ELVIS AND ILLUSTRIS1

Figure C1. Illustris-1 results for the quantities presented for the Illustris1-Dark simulation in Figures 2, 3 and 4. Upper row corresponds to the raw values from observations and simulated pairs, while the second row normalizes the same values to the mean and standard deviation on its spherically randomized counterparts.
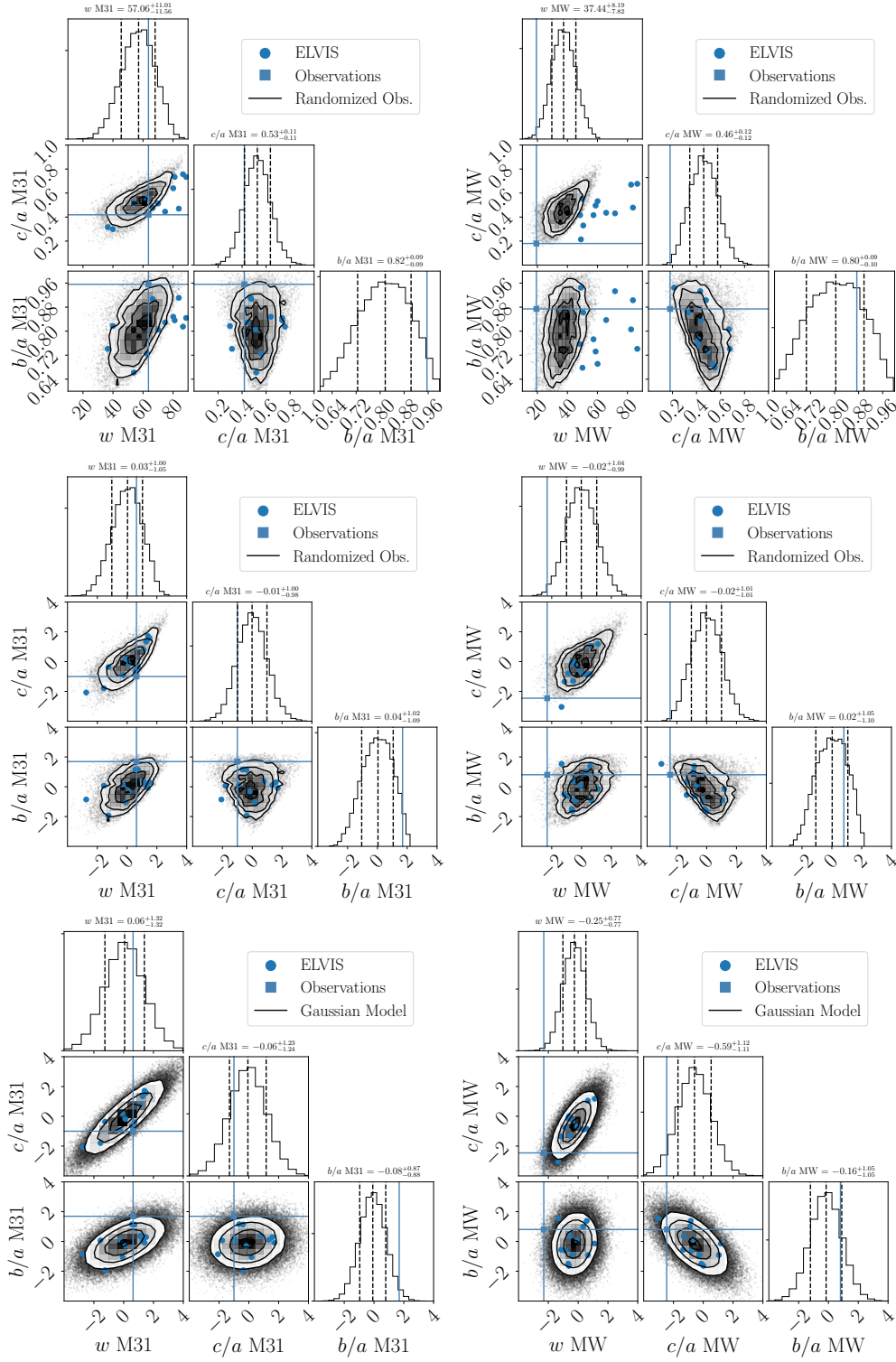
Figure C2. ELVIs results for the quantities presented for the Illustris1-Dark simulation in Figures **??**, **??**, **??**. Upper row corresponds to the raw values from observations and simulated pairs, while the second row normalizes the same values to the mean and standard deviation on its spherically randomized counterparts.